

FIRST DETERMINATION OF THE DISTANCE AND FUNDAMENTAL PROPERTIES OF AN ECLIPSING BINARY IN THE ANDROMEDA GALAXY^{1,2}

IGNASI RIBAS^{3,4}, CARME JORDI^{4,5}, FRANCESC VILARDELL⁵, EDWARD L. FITZPATRICK⁶, RON W. HILDITCH⁷, AND EDWARD F. GUINAN⁶

Draft version February 6, 2018

ABSTRACT

We present the first detailed spectroscopic and photometric analysis of an eclipsing binary in the Andromeda Galaxy (M31). This is a 19.3-mag semi-detached system with components of late-O and early-B spectral types. From the light and radial velocity curves we have carried out an accurate determination of the masses and radii of the components. Their effective temperatures have been estimated from the modeling of the absorption line spectra. The analysis yields an essentially complete picture of the properties of the system, and hence an accurate distance determination to M31. The result is $d = 772 \pm 44$ kpc ($(m - M)_0 = 24.44 \pm 0.12$ mag). The study of additional systems, currently in progress, should reduce the uncertainty in M31 distance to better than 5%.

Subject headings: binaries: eclipsing — stars: distances — stars: fundamental parameters — galaxies: individual (M31) — distance scale

1. INTRODUCTION

Accurate distance measurements to the Local Group galaxies are crucial to calibrating the Cosmic Distance Scale and to determining the age and evolution of the Universe. As major rungs on the cosmic distance ladder, these galaxies serve as calibrators for extragalactic distance indicators, such as Cepheid and RR Lyrae variables, novae, supernovae, globular clusters, etc, reaching far beyond the bounds of the Local Group (Hodge 1981). Once a Local Group galaxy's distance is known, all of its various stellar populations are available as potential standard candles. The Large Magellanic Cloud (LMC) has traditionally been used because of its proximity to the Milky Way. However, its low metallicity, and irregular geometry has posed some difficulties as illustrated by the large spread in distances derived from different methods (e.g., Gibson 2000), although recent determinations seem to reach better agreement (Alves 2004). The Andromeda Galaxy (M31) is potentially a first-class distance calibrator (Clementini et al. 2001). Its main advantages are a simple geometry, a large and diverse stellar population, and a chemical composition and morphology similar to our Galaxy and galaxies used for distance estimation (Freedman et al. 2001). Also, M31 can provide an absolute calibration of the Tully-Fisher relationship.

The distance to M31 has been estimated using a variety of methods (e.g., Holland 1998; Walker 2003; McConnachie et al. 2005) with resulting distance moduli in the range $(m - M)_0 = 24.0 - 24.5$ mag. Eclipsing binaries (EBs) are excellent distance indicators because they yield fundamental determinations of the components' radii and luminosities (Guinan et al. 1998). EBs have been used to determine accurate distances

to the LMC (e.g., Fitzpatrick et al. 2003; Ribas 2004) and SMC (e.g., Hilditch, Howarth, & Harries 2005). In addition to providing accurate distances, the fundamental stellar properties from EBs, such as masses and radii, are of great value for studying the structure and evolution of stars formed in different environments.

The first discoveries of M31 EBs (~ 60 systems) came from photographic surveys (Baade & Swope 1965 and references therein). More recently, the DIRECT group has reported about 90 new systems (see Bonanos et al. 2003 and references therein). In 1999 we undertook our own wide-field CCD photometric survey (Ribas et al. 2004) to discover and measure multi-band EB light curves with sufficient accuracy for a reliable determination of their properties. From our survey we have selected several EBs for spectroscopic follow up. Here we present the first detailed photometric and spectroscopic analysis of an EB in M31 resulting in an accurate determination of its fundamental properties and distance. This EB, designated M31VJ0044380+41292350, has an out-of-eclipse V magnitude of 19.3 and J2000.0 coordinates $\alpha = 00^{\text{h}}44^{\text{m}}38^{\text{s}}.0$, $\delta = +41^{\circ}29'23''.50$, and was reported by the DIRECT project under the identifier V12650 D31C (Stanek et al. 1999).

2. OBSERVATIONS AND REDUCTIONS

Photometry in B and V passbands of a $34' \times 34'$ field in the Northeastern quadrant of M31 was acquired with the Wide Field Camera (WFC) of the 2.5-m Isaac Newton Telescope. A total of 21 nights were allotted to our program over the course of four years (1999–2003) and ~ 265 images in each filter were obtained. Photometry in the crowded spiral arms

¹Based on observations obtained at the Gemini Observatory, which is operated by the Association of Universities for Research in Astronomy, Inc., under a cooperative agreement with the NSF on behalf of the Gemini partnership: the National Science Foundation (United States), the Particle Physics and Astronomy Research Council (United Kingdom), the National Research Council (Canada), CONICYT (Chile), the Australian Research Council (Australia), CNPq (Brazil) and CONICET (Argentina)

²Based on observations made with the Isaac Newton Telescope operated on the island of La Palma by the Isaac Newton Group in the Spanish Observatorio del Roque de los Muchachos of the Instituto de Astrofísica de Canarias

³Institut de Ciències de l'Espai – CSIC, Campus UAB, Facultat de Ciències, Torre C5 - parell - 2a, 08193 Bellaterra, Spain; e-mail: iribas@ieec.uab.es

⁴Institut d'Estudis Espacials de Catalunya (IEEC), Edif. Nexus, C/Gran Capità, 2-4, 08034 Barcelona, Spain

⁵Dept. d'Astronomia i Meteorologia, Universitat de Barcelona, Avda. Diagonal 647, 08028 Barcelona, Spain; e-mail: carme.fvilarde@am.ub.es

⁶Dept. of Astronomy & Astrophysics, Villanova University, Villanova, PA 19085, USA; e-mail: fitz@astronomy.villanova.edu, edward.guinan@villanova.edu

⁷School of Physics and Astronomy, University of St Andrews, North Haugh, St Andrews KY16 9SS, UK; e-mail: rwh@st-andrews.ac.uk

of M31 was performed using the Woźniak (2000) implementation of the Difference Image Analysis (DIA) algorithm (Alard 2000). The numerous parameters involved in the reductions were fine-tuned for best performance with the WFC images and modifications to the original code were made to improve some aspects. The resulting light curves have ~ 240 photometric measurements in V and ~ 250 in B , with individual errors of about 0.01 mag at magnitude $V = 19-20$. Full details of the reduction procedure and the resulting catalog will be given in a forthcoming publication (Vilardell, Ribas, & Jordi 2005).

To complement our photometry we considered the discovery observations from the DIRECT group (Stanek et al. 1999) with a 1.3-m telescope. Photometry was obtained mostly in the V (156 measurements) and I (54 measurements) bands, with average individual uncertainties of 0.04 mag and 0.08 mag, respectively. As shown in §3, we used the DIRECT V photometry to better constrain the orbital period and to check for consistency with our measurements (i.e., DIA vs. PSF photometry).

Spectroscopic observations were obtained with the 8-m Gemini-N telescope (program ID GN-2004B-Q-9). We used the GMOS spectrograph with a custom mask designed to deliver spectroscopy of a number of targets in a $5'5 \times 5'5$ field of view, including the EB in the present study. The instrument was set to the highest possible resolution of $R = 3744$ ($\approx 80 \text{ km s}^{-1}$ per resolution element) using a slit width of $0''.5$. The spectra cover a wavelength range of 3900–5350 Å with a sampling of about 2.6 pixels per resolution element. Because of the instrument design, there are two gaps in the spectral dispersion direction in the wavelength intervals 4367–4379 Å and 4858–4870 Å, the latter affecting the $H\beta$ Balmer line. A total of 8 spectra with exposure times of 4100 s (2×2050 s) were obtained, 4 of which were timed to cover both quadratures. The other 4 observations were taken at random phases and one of these happens to be also near quadrature. Reduction of the raw CCD frames was carried out with the IRAF Gemini package V1.7. The typical S/N of the resulting spectra is 15–30.

To derive radial velocities we considered several approaches based on both spectral disentangling and two-dimensional cross-correlation. We carried out numerous tests with the spectral disentangling codes TANGLE (Harries, Hilditch, & Howarth 2003) and KOREL (Hadrava 1995), and considering different wavelength intervals. Using a grid search method we found velocity semi-amplitudes in the ranges $K_1 = 175-200 \text{ km s}^{-1}$ and $K_2 = 260-300 \text{ km s}^{-1}$. The relatively large spread is a consequence of the noisy χ^2 surface and it was not possible to establish a definitive solution for the values of $K_{1,2}$. Alternatively, we used the TODCOR two-dimensional cross-correlation algorithm (Zucker & Mazeh 1994). We calculated individual radial velocities for each spectrum by cross-correlating with synthetic templates from Kurucz ATLAS9 models⁸ and the OSTAR2002 library (Lanz & Hubeny 2003). We considered several spectral intervals and templates of different temperatures. The various runs yielded velocities in very good mutual agreement. The resultant radial velocities for the five spectra taken near quadratures are listed in Table 1. The velocities obtained when masking out the Balmer $H\gamma$ and $H\delta$ lines, albeit of lower quality, are also in agreement.

3. MODELING OF THE LIGHT AND RADIAL VELOCITY CURVES

The light and radial velocity curves were modeled using the Wilson-Devinney (W-D) code (Wilson & Devinney 1971; Wil-

son 1990) in its 2003 version. Initial tests indicated that the system is best described by a semi-detached configuration with the secondary star filling its Roche lobe. Also, those tests suggested that the light and radial velocity curves be modeled separately because of the very few radial velocity measurements available and the possibility of a bias arising in the mass ratio of this semi-detached system. Fitting was carried out iteratively until full consistency was achieved.

In the radial velocity fit, the adjustable parameters were the orbital semi-major axis (a), the mass ratio (q) and the systemic velocity (γ). In the case of the light curves, we considered simultaneously our B and V observations, and the DIRECT V light curve (the DIRECT I -band photometry was discarded because of the poor phase coverage and low quality). The light curve fits used time as the independent variable and thus the time of minimum (T_{\min}) and the orbital period (P) were adjusted. The rest of the adjustable parameters were the orbital inclination (i), the temperature of the secondary component ($T_{\text{eff}2}$) – the temperature of the primary was adopted from §4, – the surface potential of the primary (Ω_1), and the luminosity of the primary in each passband (L_1). A circular orbit was adopted, and the gravity brightening coefficients and the bolometric albedos were set to unity in accordance with the radiative atmospheres of the components. The limb darkening coefficients (square-root law) were computed at each iteration from Kurucz ATLAS9 atmosphere models.

Convergence in the fits was reached rapidly and tests from different starting points indicated the uniqueness of the solution. It also became evident that the first quadrature is brighter than the other quadrature by about 0.025 mag in B and 0.020 mag in V . This is frequently observed in semi-detached systems with active mass transfer and may arise from the impact of a stream of matter on the accretor. We modeled this effect in W-D by including a hot spot on the primary component. Assuming such circular spot to be 40% hotter than the photosphere its predicted radius is $16^\circ \pm 1^\circ$ and located at a longitude of $277^\circ \pm 6^\circ$ (measured counter-clockwise from the line of star centers). Adding a spot in the model has little impact on the intrinsic properties of the system components but improves the quality of the fit in the out-of-eclipse region. The final r.m.s. residuals are 0.013 mag in B , 0.013 mag in V , and 0.046 mag in the DIRECT V light curve. The residuals of the radial velocities are 5.2 km s^{-1} and 4.6 km s^{-1} for the primary and secondary components, respectively. The resulting best-fitting elements are listed in Table 2, together with the fundamental stellar properties. The light and radial velocity curves with their respective fits superimposed are shown in Fig. 1. We also carried out an independent fit to the light curves with the LIGHT2 code (Hill & Rucinski 1993), obtaining results almost identical to the W-D solution.

A possible concern with light curves measured using DIA photometry is the effect of an incorrect reference flux that may cause a bias in the scale of the light curves (Michalska & Pigulski 2005). Careful tests were carried out to ensure that this was not the case. Also, the excellent agreement between the fits to our DIA photometry and the fits to the DIRECT PSF photometry strongly suggests that the flux zeropoint is correct. In addition, we ran light curve fits with a variable third light (L_3) contribution. A non-zero value (either positive or negative) of L_3 might be indicative of problems with the flux scale. This did not occur and the solutions converged to $L_3 \approx 0$. Such result has another

⁸<http://kurucz.cfa.harvard.edu/>

interesting consequence of ruling out possible blends with unresolved companions. The absence of positive L_3 is not unexpected since the light curves have the maximum possible depth ($i \sim 90^\circ$) and preclude the existence of any additional light.

4. MODELING OF THE OPTICAL SPECTRA

The photometric data available (i.e., B and V) are, by themselves, insufficient to determine the temperatures and reddening of the system. However, valuable supplemental information can be derived from the optical spectra used for the radial velocity determinations. To access this, we ran the KOREL program by fixing all the parameters to the orbital solution described in §3. This resulted in a “disentangled” spectrum for each component of the system, with a S/N of about 40. These two normalized spectra are shown in Figure 2. We then modeled this pair of spectra simultaneously using the OSTAR2002 grid of NLTE model atmospheres produced by Lanz & Hubeny (2003). The fits were constrained by the temperature ratio, surface gravities, and brightness ratio determined from the binary analysis. We solved for the constrained temperatures, a single metallicity applying to both stars, and individual values of $v \sin i$. These values are listed in Table 2 and the best-fitting models are shown in Figure 2, below each of the stellar spectra. Table 2 also lists values of M_V and $(B-V)_o$ for the system. These were produced by scaling the surfaces fluxes predicted by the OSTAR2002 models with the observed radii of the stars and performing synthetic photometry on the resultant energy distributions. The photometry was calibrated as described in Fitzpatrick & Massa (2005).

The $1-\sigma$ uncertainties in the results of the spectral analysis were determined by a Monte Carlo technique. First, we created simulations of the spectra by combining our pair of best-fit models with 50 different random noise realizations, corresponding to $S/N = 40$. For each simulated spectrum pair, we generated a simulated set of binary parameters (e.g., $T_{\text{eff}2}/T_{\text{eff}1}$), by combining the best-fit values with gaussian noise, based on the $1-\sigma$ uncertainties for each value. Finally, we fit each pair of simulated spectra as described above and adopted the standard deviations of the parameters among the 50 simulations as our uncertainties.

5. FUNDAMENTAL PROPERTIES AND DISTANCE

This is the first pair of stars in M31 for which fundamental properties have ever been directly determined. The masses and radii in Table 2 have relative uncertainties of 6–7% and 2.5–3%, respectively, which is remarkable given the faintness of the star. This opens the field of detailed investigations of stellar (single and binary) evolution models in this neighboring giant spiral galaxy. But here we focus on one of the main drivers of our program, which is the determination of the distance to the EB system. In our studies in the LMC we have adopted an approach based on the fit of the spectral energy distribution to determine the temperature, reddening, and distance to the system. At this time, such method is not applicable to this M31 binary and we have employed a different approach that uses the

available data.

The calculation of the distance is straightforward because the spectral analysis yields values for the absolute magnitudes M_V of the components and also the combined M_V of the system (see Table 2). The distance modulus follows directly from the equation: $(m-M)_o = V - M_V - A_V$. To estimate the interstellar extinction A_V , we compared the observed value of $(B-V)$ for the system with the intrinsic $(B-V)_o$ resulting from the spectral fit. Then, we computed the total extinction as $A_V = \mathcal{R}E(B-V)$ with $\mathcal{R} = 3.1 \pm 0.3$. We obtained values of $E(B-V) = 0.19 \pm 0.03$ mag and $A_V = 0.60 \pm 0.10$ mag. The overall procedure avoids the use of bolometric corrections and is self-consistent as it employs the best-fitting model atmospheres (i.e. with the appropriate $\log g$ and metallicity) to calculate the B and V magnitudes. The need for spectrophotometry could be circumvented because we derived T_{eff} from spectra and benefit from the weak temperature dependency of $(B-V)$ above ~ 30000 K to obtain an $E(B-V)$ value (although with a larger error bar).

A basic point is a reliable estimation of the error budget. With the uncertainty in M_V accounting for the full correlations of the intervening parameters, the rest of the quantities in the distance modulus equation are essentially uncorrelated. Thus, the contributions from the observed V magnitude, M_V , and A_V can be combined quadratically. From the parameters in Table 2 our calculation of the distance modulus to this M31 EB results in a value of $(m-M)_o = 24.44 \pm 0.12$ mag or, equivalently, $d = 772 \pm 44$ kpc. This distance also corresponds to the center of M31 itself because the correction due to the location of the EB is negligible ($\sim 0.3\%$). Note that the error bar accounts for the random uncertainties of the parameters but does not include a possible systematic contribution from the atmosphere models. However, we expect such systematic error to be no larger than a few percent in flux and therefore to have an effect below 0.05 mag in distance modulus.

Photometric observations carried out by the DIRECT and our own surveys have uncovered hundreds of EBs in M31, of which 10–20 are suitable for high-precision spectroscopic work (Villardell et al. 2005). Study of such EBs is underway and distance determinations for several new systems will occur in the coming years. An improved reddening/temperature estimation as well as the analysis of several EB systems will result in a direct determination of the M31 distance accurate to better than 5% or 0.1 mag in distance modulus.

Thanks are due to P. Hadrava, T. Harries, P. Woźniak, and S. Zucker for making their KOREL, TANGLE, DIA, and TODCOR codes available to us. We are grateful to the Gemini staff for the high-quality observations taken in queue mode. This program has been supported by the Spanish MCyT grant AyA2003-07736 and NSF/RUI grant no. 0507542. I. R. acknowledges support from the Spanish MEC through a Ramón y Cajal fellowship.

REFERENCES

- Alard, C. 2000, A&AS, 144, 363
 Alves, D. R. 2004, NewAR, 48, 659
 Baade, W., & Swope, H. H. 1965, AJ, 70, 212
 Bonanos, A. Z., Stanek, K. Z., Sasselov, D. D., Mochejska, B. J., Macri, L. M., & Kaluzny, J. 2003, AJ, 126, 175
 Clementini, G., Federici, L., Corsi, C., Cacciari, C., Bellazzini, M., & Smith, H. A. 2001, ApJ, 550, L109
 Fitzpatrick, E. L., & Massa, D. 2005, AJ, 129, 1642
 Fitzpatrick, E. L., Ribas, I., Guinan, E. F., Maloney, F. P., & Claret, A. 2003, ApJ, 587, 685
 Freedman, W. L., et al. 2001, ApJ, 553, 47
 Gibson, B. K. 2000, Mem. Soc. Astron. Ital., 71, 693
 Guinan, E. F., et al. 1998, ApJ, 509, L21
 Hadrava, P. 1995, A&AS, 114, 393
 Harries, T. J., Hilditch, R. W., & Howarth, I. D. 2005, MNRAS, 339, 157
 Hilditch, R. W., Howarth, I. D., & Harries, T. J. 2005, MNRAS, 357, 304

Hill, G., & Rucinski, S. M. 1993, in *Light Curve Modeling of Eclipsing Binary Stars*, ed. E. F. Milone (New York: Springer-Verlag), p. 135
 Hodge, P. W., 1981, *ARA&A*, 19, 357
 Holland, S., 1998, *AJ*, 115, 1916
 Lanz, T., & Hubeny, I. 2003, *ApJS*, 147, 225
 McConnachie, A. W., Irwin, M. J., Ferguson, A. M. N., Ibata, R. A., Lewis, G. F., & Tanvir, N. 2005, *MNRAS*, 356, 979
 Michalska, G. & Pigulski, A. 2005, *A&A*, 434, 89
 Ribas, I. 2004, *NewAR*, 48, 731
 Ribas, I., Jordi, C., Vilardell, F., Giménez, Á., & Guinan, E. F. 2004, *NewAR*, 48, 755

Stanek, K. Z., Kaluzny, J., Krockenberger, M., Sasselov, D. D., Tonry, J. L., & Mateo, M. 1999, *AJ*, 117, 2810
 Vilardell, F., Ribas, I., Jordi, C. 2005, in preparation
 Walker, A. R. 2003, in *Lecture Notes in Physics* vol. 635, *Stellar Candles for the Extragalactic Distance Scale*, eds. D. Alloin & W. Gieren (New York: Springer-Verlag), p. 265
 Wilson, R. E. 1990, *ApJ*, 356, 613
 Wilson, R. E., & Devinney, E. J. 1971, *ApJ*, 166, 605
 Woźniak, P. R. 2000, *AcA*, 50, 421
 Zucker, S., & Mazeh, T. 1994, *ApJ*, 420, 806

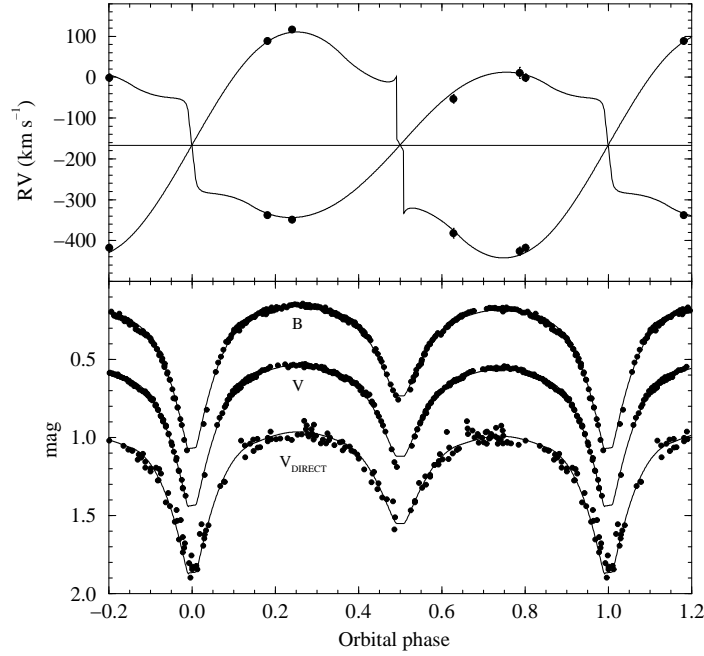


FIG. 1.— Light and radial velocity curve fits.

TABLE 1
 RADIAL VELOCITY MEASUREMENTS

HJD	Phase	RV ₁	RV ₂
2453260.90985	0.6278	-52.9±10.8	-382.0±11.7
2453262.87417	0.1812	-338.1± 7.5	88.4± 7.5
2453319.87934	0.2403	-349.1± 7.6	116.4± 6.2
2453321.82033	0.7871	10.5±13.9	-426.4±10.2
2453321.87152	0.8016	-1.1± 9.3	-417.9± 8.6

NOTE.—Units of km s⁻¹

TABLE 2
ORBITAL ELEMENTS AND FUNDAMENTAL PROPERTIES OF THE SYSTEM COMPONENTS

Parameter	Value	
P (d)	3.549694 ± 0.000010	
T_{\min} (HJD)	2452204.421 ± 0.003	
i ($^\circ$)	89.3 ± 1.8	
γ (km s^{-1})	-173 ± 4	
a (R_\odot)	33.0 ± 0.7	
$q \equiv M_2/M_1$	0.65 ± 0.03	
$T_{\text{eff}2}/T_{\text{eff}1}$	0.817 ± 0.015	
$F_2/F_1 _{B^a}$	0.487 ± 0.023	
$F_2/F_1 _{V^a}$	0.501 ± 0.022	
	Primary	Secondary
K^b (km s^{-1})	185 ± 6	285 ± 6
$r_v \equiv R/a$	0.397 ± 0.005	0.342 ± 0.005
M (M_\odot)	23.1 ± 1.3	15.0 ± 1.1
R (R_\odot)	13.1 ± 0.3	11.3 ± 0.3
$\log g$ (cgs)	3.57 ± 0.03	3.51 ± 0.04
T_{eff} (K)	$33,900 \pm 500$	$27,700 \pm 500$
$v \sin i$ (km s^{-1})	230 ± 10	145 ± 8
M_V (mag)	-5.29 ± 0.07	-4.66 ± 0.07
$(B-V)_\odot$	-0.28 ± 0.01	-0.27 ± 0.01
	System	
B^{A} (mag)	19.19 ± 0.02	
V^{A} (mag)	19.27 ± 0.02	
$[m/H]$	-0.01 ± 0.06	
$E(B-V)$ (mag)	0.19 ± 0.03	
A_V (mag)	0.60 ± 0.10	
M_V (mag)	-5.77 ± 0.06	
$(m-M)_\odot$ (mag)	24.44 ± 0.12	

^aOut-of-eclipse average: $\Delta\phi = [0.14 - 0.36] + [0.64 - 0.86]$

^bIncluding non-keplerian corrections

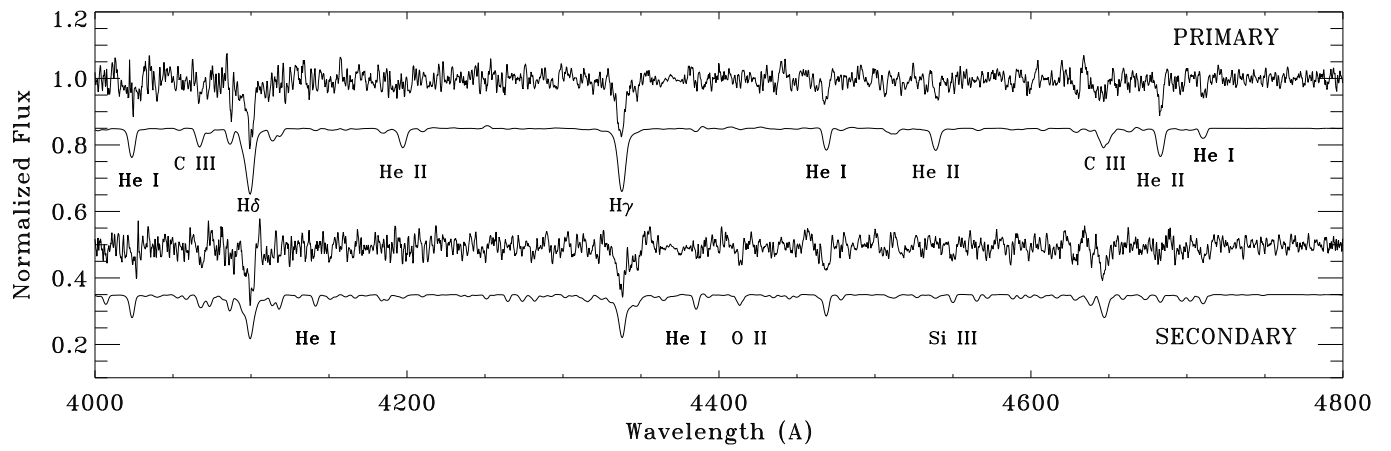


FIG. 2.— Comparison of the individual “disentangled” spectra with NLTE synthetic spectra.